Complex dynamical behavior in RCL-shunted Josephson tunnel junctions

C. B. Whan* and C. J. Lobb

Center for Superconductivity Research, Department of Physics,
University of Maryland, College Park, Maryland 20742
(Received 5 April 1995; revised manuscript received 2 October 1995)

We report an extensive numerical study of the nonlinear dynamical effects in Josephson tunnel junctions externally shunted by a resistor and an inductor in series. In the three-dimensional parameter space composed of the junction capacitance C, shunt inductance L, and the bias current I, we found the dynamics of the system extremely rich. At relatively low inductance L, we observe period doubling as well as an intermittency route to chaos. At higher values of the inductance, long chaotic transients were observed. We also studied the effect of thermal Johnson noise in the circuit and discuss the implications of our results in experiments using real Josephson tunnel junctions.

PACS number(s): 05.45.+b, 85.25.Cp, 74.40.+k, 74.50.+r

I. INTRODUCTION

In the last decade, we have witnessed a tremendous growth of research activities in chaos and nonlinear dynamics in many different branches of natural and social sciences. Josephson junctions, due to their intrinsic nonlinearity and their importance in practical applications, were among important early example systems that show chaotic behavior. Since the initial discoveries [1–5], chaos in Josephson junctions has been extensively studied in simulations, both digital [6] and analog [7], as well as in laboratory experiments [8,9] on real Josephson junctions. A recent review of the subject can be found in Ref. [10].

In most studies, a Josephson junction is described by some variation of the resistively-capacitively shunted junction (RCSJ) model, which was proposed by Stewart [11] and McCumber [12] in the late 1960's. In its simplest form, the RCSJ model uses a circuit schematically sketched in Fig. 1(a) to represent the Josephson junction. If the circuit is driven by external current I_{ext}, the circuit equation is the following:

$$C\frac{dV}{dt} + \frac{V}{R} + I_c\sin(\gamma) = I_{ext}, \tag{1}$$

$$\frac{\hbar}{2e}\frac{d\gamma}{dt} = V, \tag{2}$$

where I_c, C, and R are the junction critical current, the junction capacitance, and the junction resistance, respectively. V is the voltage and γ is the phase difference of the superconducting order parameter across the junction. As one can see from Eq. (1), the nonlinearity is due to the supercurrent term $I_c\sin(\gamma)$. If the external drive current

I_{ext} is purely dc ($I_{ext} = I_0$), we have a second-order autonomous system and therefore chaotic motion is ruled out [13]. In order to make chaos possible, we need an equation of third order or higher. One way to accomplish this is to add an ac or rf (radio-frequency) current to the external drive, i.e.,

$$I_{ext} = I_0 + I_1\sin(\omega t). \tag{3}$$

This makes Eq. (1) a second-order nonautonomous system, which can be cast into a standard third-order autonomous equation form by treating $\theta = \omega t$ as the third dynamical variable besides γ and V. The vast majority of the existing literature on chaotic behavior in Josephson junctions is based on Eqs. (1) and (3). This is partially due to the fact that this system has readily available a simple mechanical analog, namely, a pendulum driven by a combined constant and sinusoidal torque.

There are, of course, other ways to get a third-order
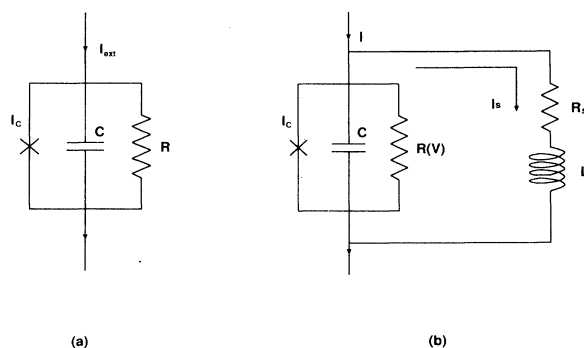

(a)   (b)

FIG. 1. Schematic sketch of (a) the RCSJ model and (b) the RCLSJ model. A Josephson tunnel junction is represented by three parallel current channels, the supercurrent $I_c\sin(\gamma)$, a capacitor C due to the overlap geometry, and a resistive channel modeling the quasiparticle leakage current.

*Present address: Department of Electrical Engineering and Computer Science, Massachusetts Institute of Technology, 77 Massachusetts Avenue, Cambridge, MA 02139. Electronic address: whan@bardeen.mit.edu

equation out of a Josephson junction circuit without resorting to an rf drive. The resistively-capacitively-inductively-shunted (*RCL*-shunted) Josephson junction, shown in Fig. 1(b), is such an example. In this circuit, we simply added a shunt branch, which is an inductance L in series with a shunt resistance R_s, to the original junction. We then current bias the entire circuit with a pure dc current $I_{ext} = I$. The equation of motion for this system is,

$$C\frac{dV}{dt} + \frac{V}{R(V)} + I_c \sin(\gamma) + I_s + I_N = I,$$

$$\frac{\hbar}{2e}\frac{d\gamma}{dt} = V, \qquad (4)$$

$$L\frac{dI_s}{dt} + I_s R_s + V_N = V,$$

where I_s is the current flowing in the shunt branch. L and R_s are, respectively, the shunt inductance and shunt resistance. I_N and V_N represent the fluctuating current noise and voltage noise that are present in the dissipative elements $R(V)$ and R_s, respectively. Here we use a voltage-dependent junction resistance, given by

$$R(V) = \begin{cases} R_N & \text{if } |V| > V_g, \\ R_{sg} & \text{if } |V| \leq V_g \end{cases} \qquad (5)$$

to reflect the existence of the gap voltage $V_g = 2\Delta/e$ in the tunnel junction *I-V* curve. R_N and R_{sg} are the junction normal-state resistance and the subgap resistance, respectively.

Theoretical study of chaos in a system similar to the present one was reported by Marcus, Imry, and Ben-Jacob [14]. Miracky, Clarke, and Koch [9] measured noise and found experimental evidence for chaotic motion in this system. The same group also did analog simulations and mapped out a very rough parameter space indicating the regions where different types of dynamics occur. Along those lines, there is also the experiment by Smith *et al.* [15] who measured the linewidth of a voltage-controlled Josephson oscillator and explained the linewidth broadening in terms of chaos.

In a previous paper [16], we reported our experimental investigation of the *RCL*-shunted Josephson tunnel junctions. By comparing our experimental dc *I-V* characteristics with numerical simulations, we found that the parameter values of our samples fell in a region where either Josephson oscillations or subharmonic relaxation oscillations dominate the dynamics. In this paper we present more numerical simulation results, which cover a wider range of parameter space and some details of the nonlinear dynamical behavior in this system. In the parameter ranges that have been explored previously, our results are in agreement with the analog simulations of Miracky, Clarke, and Koch [9], although we have discovered some interesting dynamical details in this regime. Among the new results in this paper are the existence of chaotic transients in a wide range of parameter space and the effects of thermal Johnson noise. We also discuss the implications of our work in real Josephson junction experiments.

The circuit model we use here is the same as Ref. [16]. The dynamical equation, Eq. (4), can be put into the following standard form for nonlinear dynamical analysis:

$$\frac{d\mathbf{x}}{d\tau} = \mathbf{F}(\mathbf{x}), \qquad (6)$$

where

$$\mathbf{x} = \begin{bmatrix} x_1 \\ x_2 \\ x_3 \end{bmatrix} = \begin{bmatrix} \gamma \bmod 2\pi \\ \frac{V}{I_c R_s} \\ \frac{I_s}{I_c} \end{bmatrix},$$

$$\mathbf{F}(\mathbf{x}) = \begin{bmatrix} x_2 \\ \frac{1}{\beta_C}[i - gx_2 - \sin(x_1) - x_3] \\ \frac{1}{\beta_L}(x_2 - x_3) \end{bmatrix},$$

and the normalized time $\tau = \omega_c t$, with $\omega_c = 2eI_c R_s/\hbar$. Notice that we neglected the noise terms I_N and V_N here for simplicity. We will continue to do so until Sec. III, where we will explicitly discuss the noise effects.

We notice that Eq. (6) contains four parameters, the Stewart-McCumber parameter $\beta_C = 2eI_c R_s^2 C/\hbar$, the dimensionless inductance $\beta_L = 2eI_c L/\hbar$, the external dc bias $i = I/I_c$, and the tunnel junction conductance $g = R_s/R(V)$. Therefore we have a four-dimensional parameter space to explore, which apparently is a formidable task. Since our original interest was motivated by our experimental study of the effects of shunt inductance in this system [16], we will first discuss the bifurcation diagrams by changing the parameter β_L while keeping the other parameters fixed at values that are appropriate for the samples we used in our experiment. Later, we will also look at some bifurcation diagrams where we use β_C or i as the control parameters. We will not change g in this paper (i.e., we will deal with a three-dimensional parameter space), its value will be determined, according to Eq. (5), by

$$g = \begin{cases} R_s/R_N & \text{if } |x_2| > V_g/(I_c R_s), \\ R_s/R_{sg} & \text{if } |x_2| \leq V_g/(I_c R_s), \end{cases} \qquad (7)$$

with the values of all the relevant variables appropriate for a typical $Nb/Al_2O_3/Nb$ tunnel junction. In particular, for the samples that we have studied in Ref. [16], at temperature $T = 7.60$ K, $V_g/(I_c R_s) \approx 6.9$, and $R_s/R_{sg} \approx 0.0478$.

In practical circuit design, it is useful to have a detailed knowledge about the dynamical behavior of the system in different parameter ranges, so that one can avoid certain undesirable regions in the parameter space to optimize the circuit performance. To this end, bifurcation diagrams are very useful tools for visualizing the global dynamical behavior of a system under design. In this paper we will use bifurcation diagrams extensively to illustrate various oscillations that are present in our system. The voltage bifurcation diagrams are obtained by recording the local maxima in the voltage time series [13].

The quantitative criterion for a time series to be chaotic is the positivity of one of its Lyapunov expo-

nents (there are three of them, for our three-dimensional system). In this paper, we will compute only the largest Lyapunov exponent, which is sufficient to distinguish a chaotic signal from a periodic signal. Assume we perturb the system trajectory at $\tau = 0$ by $\delta\mathbf{x}(0)$, then we expect,

$$\left|\frac{\delta\mathbf{x}(\tau)}{\delta\mathbf{x}(0)}\right| \sim e^{\lambda_1 \tau}, \qquad \tau \to \infty \tag{8}$$

and the largest Lyapunov exponent λ_1 is given by

$$\lambda_1 = \lim_{\tau \to \infty} \lambda(\tau), \tag{9}$$

$$\lambda(\tau) \equiv \frac{1}{\tau}\ln\left|\frac{\delta\mathbf{x}(\tau)}{\delta\mathbf{x}(0)}\right|. \tag{10}$$

In order to avoid computer overflow, Benettin *et al.* [17] suggested that one should normalize $|\delta\mathbf{x}|$ frequently and keep track of the growth (or shrinkage) factor, i.e.,

$$\lambda(\tau) = \frac{1}{n\Delta\tau}\sum_{i=0}^{n-1}\log\left|\frac{\delta\mathbf{x}[(i+1)\Delta\tau]}{\delta\mathbf{x}(i\Delta\tau)}\right|. \tag{11}$$

Here we divided τ into n subintervals ($\tau = n\Delta\tau$). In the limit $n \to \infty$, Eq. (11) gives us λ_1. In practice λ_1 is always approximated by some $\lambda(\tau)$ with a large finite τ. As we can see from the definition, Eqs. (9) and (10), if $\lambda_1 > 0$, any error will be amplified exponentially, which is a characteristic often used to define chaos.

II. BIFURCATION DIAGRAMS: AN OVERVIEW OF THE GLOBAL DYNAMICS

In Fig. 2, we show a bifurcation diagram obtained using the local maxima method, while changing the control parameter β_L in the range $0 \le \beta_L \le 10$. The other parameters are held constant at values $\beta_C = 0.707$ and
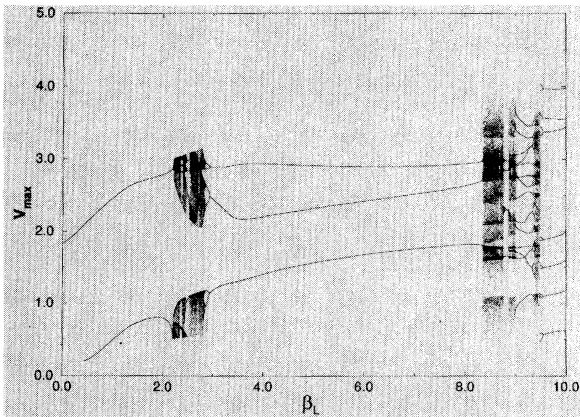
$i = 1.20$. At $\beta_L = 0$, the junction is shunted by a pure resistor and the usual RCSJ model applies. In this limit, we know the dynamics are pure ac Josephson oscillations and the bifurcation diagram shows a single dot indicating periodic motion. Also from a dynamical systems point of view, zero-inductance value ($\beta_L = 0$) means the system is reduced to a second-order system [see Eqs. (4)–(6)], therefore chaotic motion is necessarily ruled out [13]. As we increase the shunt inductance value gradually from zero, the system goes through some regions where the dynamics appear to be quite complex.

In order to reveal some more details of the dynamics in this complicated regime, we focus on the region $2 \le \beta_L \le 3$. The result is shown in Fig. 3, together with the largest Lyapunov exponent λ_1 in the same parameter region. We see that for $\beta_L < 2.198$, the motion is periodic, which is indicated by two distinct dots for a given value of β_L in the bifurcation diagram [Fig. 3(a)] as well as the zero value for the largest Lyapunov exponent [Fig. 3(b)]. The system becomes chaotic at $\beta_L \approx 2.198$. A closer look at the time series and the Poincaré map (not shown), right before and after the transition shows that the transition is that of a type I intermittency via saddle-node bifurcation [18]. As the β_L value is increased further, we see fully developed chaotic motions occasionally interrupted by periodic windows. Looking from the high β_L end of Fig. 3(a), we see a period-doubling bifurcation route to chaos.

Notice the period doublings we see here are different from that in a driven system [such as the system described by Eqs. (1) and (3)] where one has a natural fundamental frequency, the drive frequency ω. There, all the

FIG. 2. A bifurcation diagram with β_L as the control parameter. The other parameters are fixed at $i = 1.20$ and $\beta_C = 0.707$.
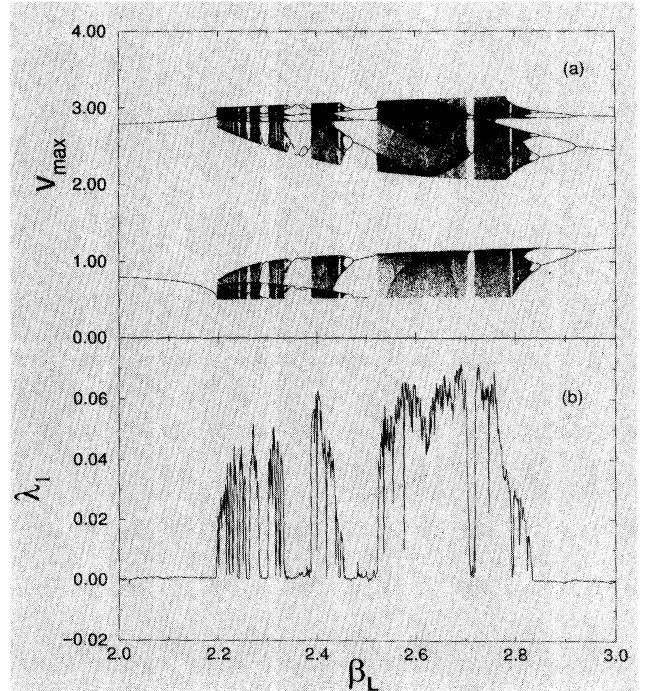

FIG. 3. (a) Detail of the bifurcation diagram of Fig. 2. (b) The corresponding largest Lyapunov exponent.

period doublings are in reference to ω, while here we do not have such a natural time scale built in. What turns out to be important is the Josephson frequency, defined by

$$\omega_J = \frac{2e}{\hbar}\bar{V} = \omega_c \bar{x}_2. \tag{12}$$

Here the overbar denotes time average. The period-doubling bifurcation also manifests itself as subharmonic peaks in the power spectra (not shown) at frequencies,

$$\frac{\omega}{\omega_J} = \frac{1}{2^n}, \tag{13}$$

with n being an integer. This is drastically different from

the usual behavior at higher β_L, where chaos is generally absent and one sees subharmonic relaxation oscillations at frequencies [16,19]

$$\omega = \omega_J/n, \tag{14}$$

and generally, $n < \beta_L$.

By constructing bifurcation diagrams with a wider range of β_L values, we found that chaos is generally absent at high β_L, roughly $\beta_L > 50$. In this regime, the dynamics is dominated by relaxation oscillations [20–22] In an intermediate range, roughly $10 < \beta_L < 50$, the dynamics get complicated by the presence of chaotic transients. We will discuss chaotic transients in the next section.

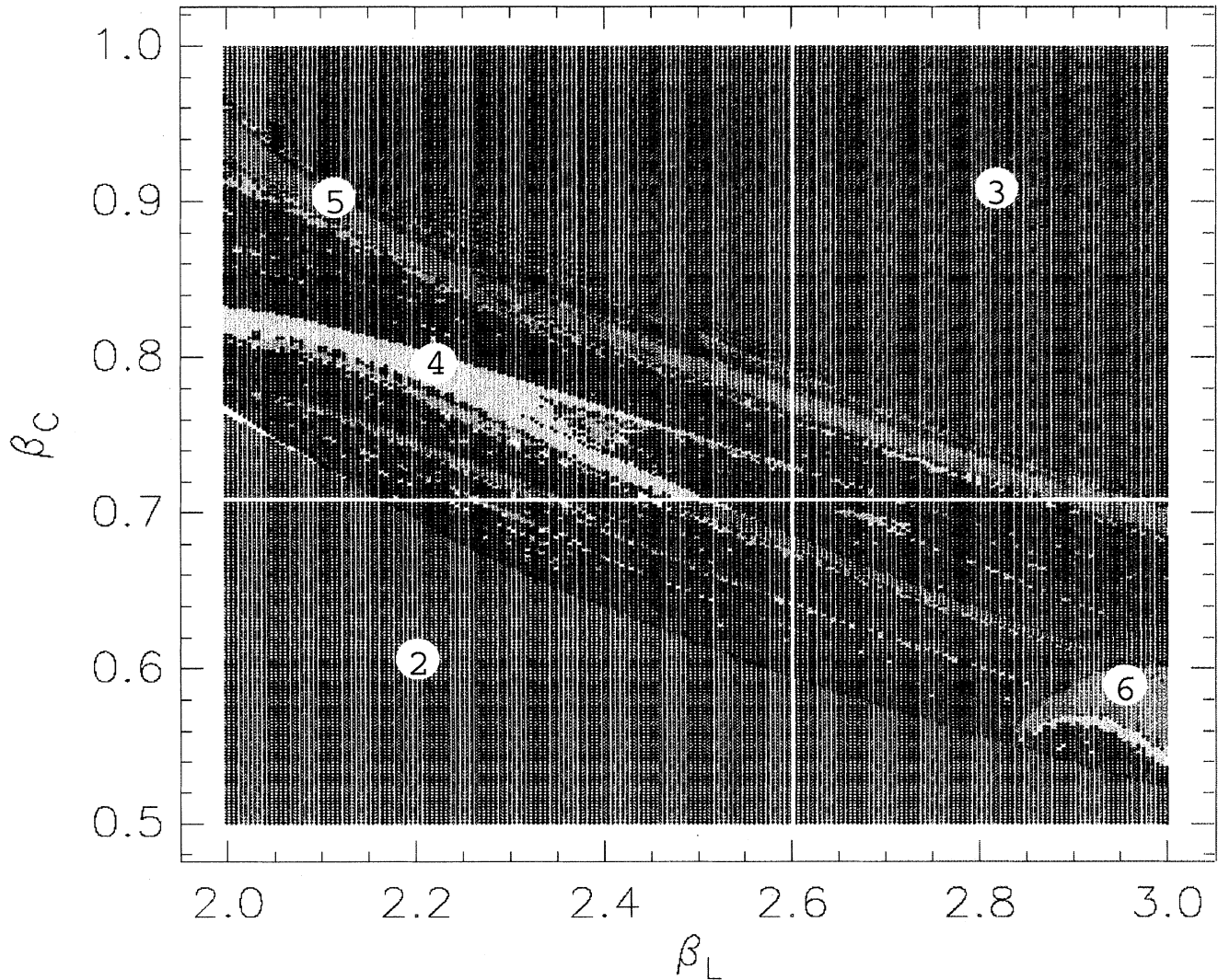In the bifurcation diagrams shown in Fig. 2 and

FIG. 4. A two-dimensional generalization of the bifurcation diagrams. Here the bias current is fixed at $i = 1.20$ and the other two parameters β_L and β_C are varied on a 250×200 grid. The color code for several low-periodicity solutions are indicated by the numbers in small circles. All solutions with periodicity higher than 20, including chaotic solutions, are marked black. The horizontal white line corresponds to the bifurcation diagram of Fig. 3(a).

Fig. 3(a), we selected β_L as our control parameter. The other two parameters β_C and i were held constant. The reason we chose β_L is simply because our initial interests were motivated by our experimental conditions, as we mentioned earlier. From a more general point of view, we could choose any one of the three available parameters, i, β_C, and β_L, while holding the remaining two parameters constant. Moreover, since we have a three-dimensional parameter space, the dynamics of our system would depend on the location of our operating point in this three-dimensional space. Bifurcation diagrams obtained by changing one of the parameters provide information about the dynamics only along short line segments parallel to the corresponding axis in the three-dimensional parameter space. We can visualize the system dynamics more efficiently by generalizing the bifurcation diagrams in the following way. We can imagine cutting the three-dimensional parameter space with a plane and examine the dynamics in a rectangular region on this plane. We divide this rectangle into a two-dimensional grid and use color coding at each node of the grid to denote its periodicity (in the rest of this section, we will loosely use the term "periodicity" to refer to the number of peaks in the voltage wave form, which should not be confused with the *time* period of the voltage oscillations).

Figure 4 is such a construction. Here we fix the bias current at $i = 1.20$. The other two parameters, β_L and β_C, are varied on a 250×200 grid. In this plot we illustrate only some low periodicity solutions. The periodicity-color correspondence is marked by the numbers in small white circles. Any point with periodicity greater than 20 is marked black as are the points whose periodicity needs to be determined with higher accuracy [23,24] In particular, the chaotic solutions are buried in those dark regions.

The bifurcation diagram in Fig. 3(a) corresponds to the white horizontal line in Fig. 4. Similarly, if we were to construct a bifurcation diagram using β_C as the control parameter, it would be a vertical line. In this sense, we can think of plots like Fig. 4 as generalizations of the one-dimensional bifurcation diagrams. This observation has important practical implications. Although we know chaos is absent in the zero-inductance (i.e., $\beta_L = 0$) circuit, it becomes a possible solution for relatively small ($\beta_L \geq 1$) inductance. Furthermore, the chaotic solutions in general cannot be "tuned away" by simply changing the inductance alone. One needs to look at the full parameter space and decide the optimal operating region and subsequently design *all* the relevant parameters in the desired regime in order to avoid chaos. While it is difficult to imagine a three-dimensional construction illustrating the complete dependence of the system dynamics on all the parameters, a two-dimensional construction such as Fig. 4 is certainly a big step forward.

The parameter space structure of multiparameter nonlinear dynamical systems is an interesting research subject on its own. For example, Gallas [25] has studied the Henon map and other discrete maps with two-dimensional parameter spaces, and found "shrimplike" clusters of period k (where k is an integer) orbits and

their infinite period-doubling sequences that extend into the surrounding chaotic "sea". Our parameter space is three dimensional and whether the shrimplike structures exist on a two-dimensional cross section of it remains to be seen. Clearly, the structure of parameter space in *RCL*-shunted Josephson junction needs further study, both from the viewpoints of nonlinear dynamics and practical design of devices.

III. CHAOTIC TRANSIENTS AND EFFECTS OF THERMAL NOISE

A chaotic transient is a metastable stage in the trajectory of a nonlinear dynamical system before it eventually converges to its true attractor. During the transient period, the trajectory is often indistinguishable from a true chaotic trajectory. Chaotic transients were first observed numerically in the study of Lorenz systems [26,27], and subsequently there have been reports on experimental observations of chaotic transients in various physical and biological systems. More details can be found in the review paper by Tél [28].

We found in our system, Eq. (4), chaotic transients are fairly common for intermediate range values of β_L. In Fig. 5(a), we show a voltage time series at parameter values, $\beta_L = 29.215$, $\beta_C = 0.707$, and $i = 1.25$. We
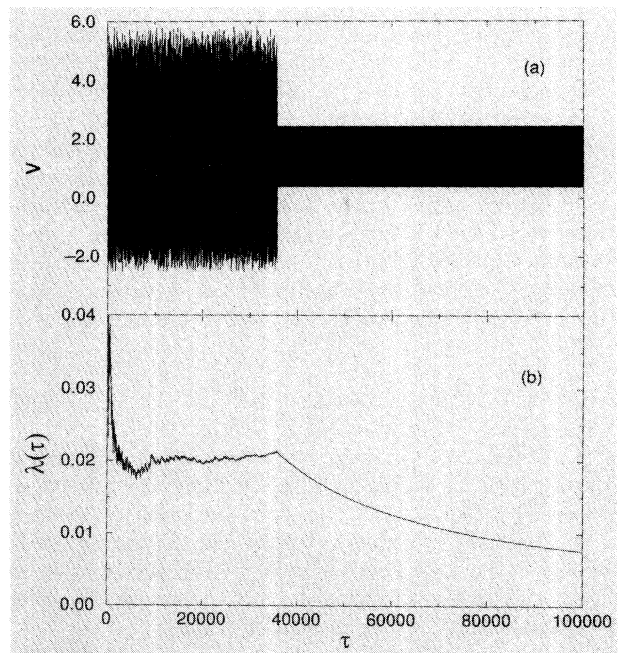

FIG. 5. A chaotic transient is illustrated here in the voltage wave form (a), and also by the approximate Lyapunov exponent $\lambda(\tau)$ (b). The parameter values are $\beta_L = 29.215$, $\beta_C = 0.707$, and $i = 1.25$. The lifetime of the chaotic transient is $\tau_{tr} \approx 36\,000$. Notice that as soon as the trajectory reaches the periodic attractor, $\lambda(\tau)$ starts to decay as $1/\tau$, eventually giving $\lambda_1 = 0$.

see that the voltage starts off with a very irregular and seemingly chaotic motion but at $\tau = \tau_{\rm tr} \approx 36\,000$ it suddenly switches back to a regular periodic motion. Here we use $\tau_{\rm tr}$ to denote the lifetime of the chaotic transient. The periodic solution, in this case a regular Josephson oscillation, is the real attractor, i.e., once the system is in this oscillation mode, it stays there indefinitely. We have followed the wave form up to 5×10^5 time steps, and never saw it change again.

Transient chaos can also be illustrated by computing the Lyapunov exponents. In Fig. 5(b), shown together with the time series is the approximate (maximum) Lyapunov exponent $\lambda(\tau)$ as a function of time τ. According to the definition, Eqs. (9) and (10), in a true chaotic trajectory $\lambda(\tau)$ should approach the constant value $\lambda_1 > 0$ as we increase τ, indicating exponential magnification of errors. On the other hand, if the trajectory is periodic, the error will either shrink exponentially fast (if the perturbation is normal to trajectory) or stay unchanged (if perturbation is tangential to the trajectory). Since we are computing *the largest* Lyapunov exponent for perturbation in arbitrary directions, we should get a zero λ_1 value for periodic solutions [29]. When there is a chaotic transient in the trajectory, we see from Fig. 5(b) that $\lambda(\tau)$ starts off with a fluctuating part and tends to converge to a positive value 0.02 for $\tau < \tau_{\rm tr}$. But as soon as the transient is over (i.e., for $\tau > \tau_{\rm tr}$), the amplification of error ceases and $\lambda(\tau)$ starts to decrease as $1/\tau$, giving $\lambda_1 = 0$ in the $\tau \to \infty$ limit as we expected.

The lifetime of the chaotic transients depends sensitively on the initial conditions. If we repeat the simulation of Fig. 5(a) with identical parameter values but with a different initial condition we get a different value for the transient lifetime $\tau_{\rm tr}$. If we consider an ensemble consisting of $N(0)$ trajectories, each starting with a different initial condition, the lifetimes of transients in each trajectory are different. Therefore the number of trajectories remaining in the transient state will decrease as time evolves, as there will be more and more trajectories that leave the transient and approach the periodic attractor. At time τ, the number of trajectories remaining in the transient state is expected to follow the decay law [27]

$$N(\tau) = N(0)e^{-\tau/\langle \tau_{tr} \rangle}. \tag{15}$$

In Fig. 6, we show that in our system Eq. (15) holds rather nicely. This figure is obtained from an ensemble of $N(0) = 393$ trajectories. The average transient lifetime $\langle \tau_{tr} \rangle$ is obtained by simply taking the algebraic mean of all 393 $\tau_{\rm tr}$'s [note there are no fitting parameters in Eq. (15)]. The simulation result is shown by the solid curve and the dashed line is from Eq. (15).

Up until now, all our simulations have neglected the effect of noise. Real measurements are always done at a finite temperature, and there will always be some interference from the environment. This includes instrument noise, thermal Johnson noise due to the resistors in the circuit, and shot noise in the quasiparticle tunneling current. We will now discuss the noise effects in our system limiting ourselves only to the thermal Johnson noise,
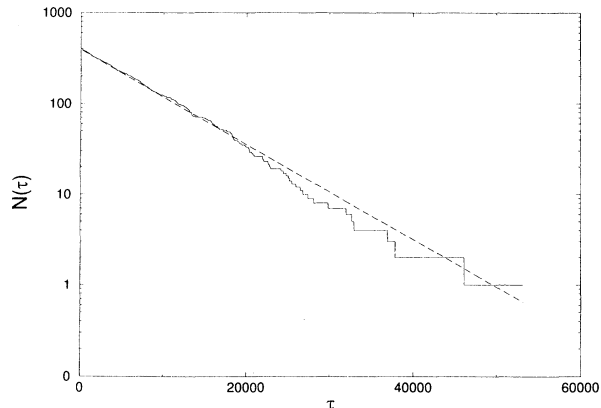

FIG. 6. The decay of 393 trajectories starting from randomly chosen initial conditions with identical parameter values. The number of trajectories remaining in the chaotic transient state decays exponentially, according to Eq. (15), due to finite lifetime of the transient chaotic states. The solid line is the simulation result and the dashed line is Eq. (15). The average lifetime of all transients is $\langle \tau_{tr} \rangle = 8293$. The parameter values are $\beta_L = 29.215, \beta_C = 0.707$, and $i = 1.25$.

which is expected to be the dominant noise source at low voltages [19].

We treat the noise terms in Eq. (4) using a method introduced by Tesche and Clarke [30], where the noise voltage and noise current are represented by Gaussian distributed random forces, with the distribution widths appropriate for the white noise background for the given temperature. The correlation functions for the noise terms are given, in reduced dimensionless units, by

$$\langle i_N(\tau)i_N(\tau') \rangle = 2g\Gamma\delta(\tau - \tau'),$$

$$\langle v_N(\tau)v_N(\tau') \rangle = 2\Gamma\delta(\tau - \tau'), \tag{16}$$

where $\Gamma = 2ek_BT/(I_c\hbar)$ is the relative strength of the thermal fluctuations at temperature T. For the junctions studied in [16], $I_c = 0.275$ mA at $T = 7.60$ K, which corresponds to $\Gamma = 1.16 \times 10^{-3}$.

Figure 7 shows the effect of thermal noise on the bifurcation diagrams at four different temperatures. At the top of Fig. 7 is a portion of the bifurcation diagram of Fig. 3(a) and the three diagrams below it are the same diagram in the presence of increasing level of thermal noise at $T = 0.076, 0.76$, and 7.60 K, corresponding to $\Gamma = 1.16 \times 10^{-5}, 1.16 \times 10^{-4}$, and 1.16×10^{-3}. Most Josephson devices are expected to operate at liquid-helium temperature (4.2 K) or higher. We see from Fig. 7, at this temperature range, bifurcation diagrams that we saw in the last sections are completely obliterated by the noise effect. In order to resolve major structures in the bifurcation diagrams, one needs to lower the temperature by at least two orders of magnitude (i.e., < 100 mK). This requires special cooling techniques, such as a dilution refrigerator [31]. We note that our results here

are consistent with previous studies of noise effects in discrete maps [32] and driven pendulum [33].

Another interesting phenomenon is the profound effect that the noise has on the chaotic transients. Grebogi, Ott, and Yorke [34] argued that the effect of noise on chaotic transient will be to increase the average lifetime of the transient. Kautz [35] has studied the noise effect in rf-driven Josephson junctions and observed that even with a very low level of noise the chaotic transients effectively turn themselves into permanent chaotic states, which he calls noise-induced chaos.

In Fig. 8, we show the effect of noise on two chaotic transient states in our system using the approximate Lyapunov exponents. Here $\lambda(\tau)$'s are computed along the noisy trajectory using same initial conditions at different levels of noise. At $i = 1.20$ [Fig. 8(a)], even a noise level as low as $\Gamma = 1.16 \times 10^{-5}$ (corresponding to $T = 7.6$ mK, which is close to the practical limit of modern dilution refrigerators) is sufficient to drive the chaotic transient

into chaos, indicated by the converging of $\lambda(\tau)$ to a positive value. We have repeated the $\lambda(\tau)$ calculation several times using different initial conditions at this lowest noise level ($T = 0.0076$ K), we saw no sign of it switching to a periodic motion (as it does for $T = 0$) for time $\tau < 200\,000$. At $i = 1.25$ [Fig. 8(b)], however, the situation is slightly different. Noise-induced chaos is absent in this case until the noise level reaches some minimum. It is obvious from Figs. 8(a) and 8(b), that the minimum noise required for the noise-induced chaos to occur depends upon the system parameters, as we might have anticipated.

Chaotic transients and their behavior in the presence of noise have important implications in laboratory experiments on Josephson devices. Typical Josephson junctions operate at a frequency range of several hundred GHz, corresponding to time scale of about 1 ps. There is no instrument (such as an oscilloscope) fast enough that one can use to monitor the dynamics of the circuit in real
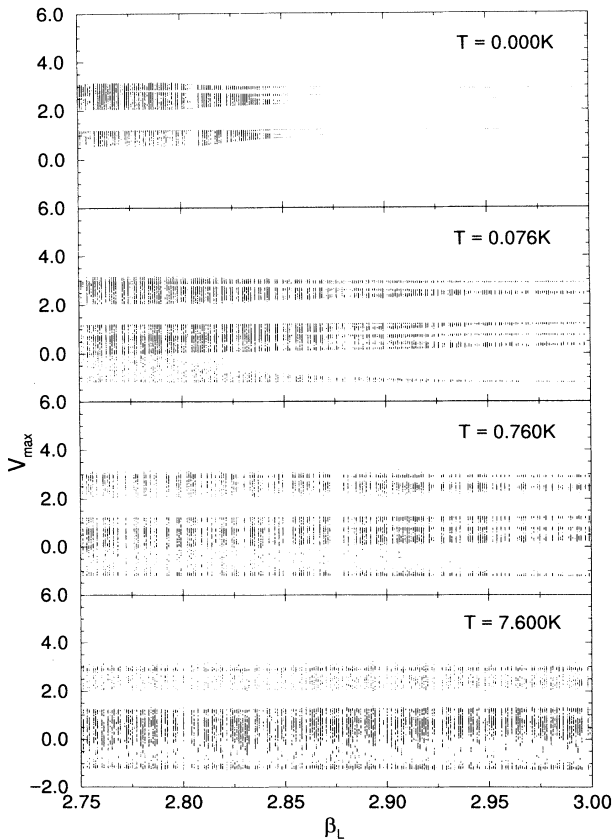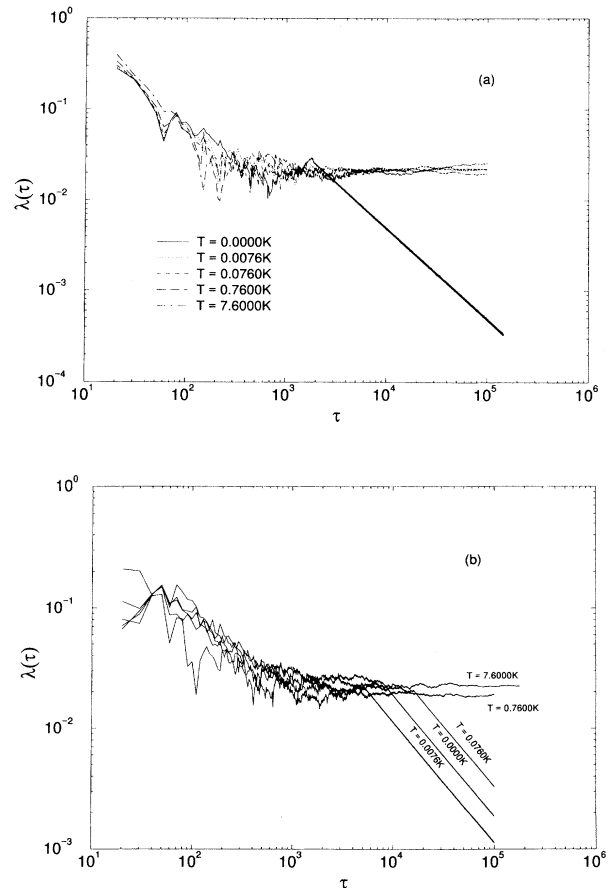

FIG. 7. A section of the bifurcation diagram in Fig. 3 affected by increasing levels of noise. From top to bottom, the temperature values are $T = 0.0, 0.076, 0.76$, and 7.6 K. It is clear from this picture that most details of the bifurcation diagrams that we showed earlier will be completely obliterated by thermal fluctuations even at liquid-helium temperature ($T = 4.2$ K).

FIG. 8. The noise-induced chaos. The $\lambda(\tau)$-τ plot is shown here for five different temperatures for $i = 1.20$ (a) and $i = 1.25$ (b). In (a), chaotic transient that existed at $T = 0$ K turns itself into permanent chaos for all four finite temperature values. In (b), however, we see that a minimum level of noise is required for noise induced chaos to occur. The other parameter values are $\beta_L = 29.215$ and $\beta_C = 0.707$.

time.

Due to such a handicap, one often has to rely on numerical solutions of the corresponding circuit equations to gain knowledge of the detailed dynamics. The numerical model is usually tested against the experiment by requiring some averaged properties of the circuit (such as a current-voltage characteristic), which are available both numerically and experimentally, to agree with one another. One should note, though, the averages done in experiments and in numerical simulations are often at very different time scales. For example, a modern digital voltmeter will average on a time scale of about 1 ms or even longer. In our normalized time unit, taking a typical value $\omega_c = 10^{11}$ Hz, this means an averaging time of $\tau_{\text{ave}} = 10^{-3}$ s $\times 10^{11}$ Hz$= 10^8$. Assuming the integration time step is $\Delta\tau = 0.01$, one needs to integrate and average the circuit differential equations for around 10^{10} time steps for every single point in the I-V characteristic. This is certainly impractical for most purposes. In practice, most numerical averaging is done on a time scale of about $\tau_{\text{ave}} = 1000$, which corresponds to 10^{-8} s in real time. Therefore the typical averaging time in a voltmeter and a simulation differ by as much as 5 orders of magnitude. Normally it is not a concern, since we do not expect a voltage signal of 1 Thz averaged over 1 ms to be much different from the same signal averaged over 1 ns. Such is not the case, however, if chaotic transients are present. We saw earlier that the lifetime of these chaotic transients can be as long as $\tau_{\text{tr}} \sim 10^4 - 10^5$. It is easy to imagine a situation where the simulation averaging is done on a transient chaotic state while the experimental averaging is on the true attractor, simply due to their vastly different time scales. The situation is further complicated by thermal noise, which could push *some* of the chaotic transients into permanent chaotic states (noise-induced chaos). With these difficulties, one certainly cannot use the agreement of the two averaging schemes to check the validity of the numerical model.

IV. CONCLUSION

In conclusion, we have numerically studied the global dynamical behavior of RCL-shunted Josephson junctions. Complicated solutions, such as chaos, exist at relatively low inductance values of the junction. One should be aware of this in practical circuit design, since the inductance from the shunt can easily put the circuit into the chaotic region unless special care is taken to reduce the inductance. At higher values of the inductance the dynamics is complicated by the existence of chaotic transients. At even higher inductance, the relatively simple relaxation oscillations dominate the dynamics. Complicated dynamical behavior is also revealed by changing circuit parameters other than the inductance and the structure of the parameter space where different types of dynamics occur are quite complicated. We found that the period-doubling bifurcations that existed in the absence of noise are severely obliterated by thermal noise at normal operating temperature of these devices. We also observed noise-induced chaos in our system, where the chaotic transient effectively turns itself into permanent chaos in the presence of noise. A parameter-dependent minimum noise level seems to be required for noise-induced chaos. Finally, we note that the existence of chaotic transients and their complex noise behavior pose some difficulty in comparing numerical simulations with laboratory experiments, due to the drastically different time scales involved in these two approaches.

[1] B. A. Huberman, J. A. Crutchfield, and N. H. Packard, Appl. Phys. Lett. **37**, 750 (1980).

[2] Y. Braiman, E. Ben-Jacob, and Y. Imry, in *SQUID 80*, edited by H. D. Hahlbohm and H. Lubbig (de Gruyter, Berlin, 1980), p. 783.

[3] E. Ben-Jacob, Y. Braiman, R. Shainsky, and Y. Imry, Appl. Phys. Lett. **38**, 822 (1981).

[4] R. L. Kautz, J. Appl. Phys. **52**, 3528 (1981).

[5] N. F. Pedersen and A. Davidson, Appl. Phys. Lett. **39**, 830 (1981).

[6] For an early survey, see, for example, R. L. Kautz and R. Monaco, J. Appl. Phys. **57**, 875 (1985).

[7] D. D'Humieres, M. R. Beasley, B. A. Huberman, and A. Libchaber, Phys. Rev. A **26**, 3483 (1982).

[8] M. Octavio and C. Readi Nasser, Phys. Rev. B **30**, 1586 (1984).

[9] Robert F. Miracky, John Clarke, and Roger H. Koch, Phys. Rev. Lett. **50**, 856 (1983); Robert F. Miracky, Ph.D. thesis, University of California, Berkeley, 1984.

[10] U. Küger, J. Kurkijärvi, M. Bauer, and W. Martienssen, in *Nonlinear Dynamics in Solids*, edited by H. Thomas (Springer-Verlag, Berlin, 1992).

[11] W. C. Stewart, Appl. Phys. Lett. **12**, 277 (1968).

[12] D. E. McCumber, J. Appl. Phys. **39**, 3113 (1968).

[13] For a general reference on the subject see the text by Edward Ott, *Chaos in Dynamical Systems* (Cambridge University Press, Cambridge, 1993).

[14] P. M. Marcus, Y. Imry, and E. Ben-Jacob, Solid State Commun. **41**, 161 (1982).

[15] A. D. Smith, R. D. Sandell, A. H. Silver, and J. F. Burch, IEEE Trans. Magn. **MAG-23**, 1269 (1987).

[16] C. B. Whan, C. J. Lobb, and M. G. Forrester, J. Appl.

Phys. **77**, 382 (1995); C. B. Whan, Ph.D. thesis, University of Maryland, 1995.

[17] G. Bennetin, L. Galgani, A. Giorgilli, and J.-M. Strelcyn, Meccanica **15**, 21 (1980).

[18] Y. Pomeau and P. Manneville, Commun. Math. Phys. **74**, 189 (1980).

[19] K. K. Likharev, *Dynamics of Josephson Junctions and Circuits* (Gordon and Breach, New York, 1986).

[20] J. E. Zimmerman and A. H. Silver, Phys. Rev. Lett. **19**, 14 (1967); D. B. Sullivan, Robert L. Peterson, V. E. Kose, and J. E. Zimmerman, J. Appl. Phys. **41**, 4865 (1970). Also see Y. Taur and P. L. Richards, *ibid.* **46**, 1793 (1975).

[21] F. L. Vernon, Jr. and R. J. Pedersen, J. Appl. Phys. **39**, 2661 (1968).

[22] N. Calander, T. Claeson, and S. Rudner, Appl. Phys. Lett. **39**, 504 (1981); Phys. Scr. **25**, 837 (1982).

[23] There are two reasons for this simplification. First it is not always easy to find many colors that are visually strikingly distinct. Second, higher periodicity orbits that are created via period-doubling bifurcations usually occupy very narrow regions in the parameter space and they get narrower very fast as they bifurcate to even higher periodicity solutions [24], therefore even if one had a color pallette that solved the visual contrast problem we would still be limited by spatial resolution.

[24] M. J. Feigenbaum, Los Alamos Science **1**, 4 (1980).

[25] Jason A. C. Gallas, Phys. Rev. Lett. **70**, 2714 (1993); Physica (Amsterdam) **202A**, 196 (1994), and references therein.

[26] J. L. Kaplan and J. A. Yorke, Commun. Math. Phys. **67**, 93 (1979).

[27] J. A. Yorke and E. D. Yorke, J. Stat. Phys. **21**, 263 (1979).

[28] T. Tél, in *Direction in Chaos*, edited by Bai-Lin Hao, D. H. Feng, and J.-M. Yuan (World Scientific, Singapore, 1991), Vol. 3.

[29] H. Haken, Phys. Lett. **94A**, 71 (1983).

[30] C. D. Tesche and J. Clarke, J. Low Temp. Phys. **29**, 301 (1977).

[31] Of course, the noise effect is not the only factor that limits us from observing bifurcation diagrams. The typical time scale of a Josephson device, being on the order of 1 ps, is the major obstacle in our ability to observe any dynamical details in these systems in a laboratory experiment. On the other hand, high speed is exactly what makes these devices so attractive in practical applications.

[32] J. P. Crutchfield, J. D. Farmer, and B. A. Huberman, Phys. Rep. **92**, 45 (1982).

[33] J. C. Sommerer, E. Ott, and C. Grebogi, Phys. Rev. A **43**, 1754 (1991).

[34] C. Grebogi, E. Ott, and J. A. Yorke, Ergod. Theor. Dyn. Syst. **5**, 341 (1985).
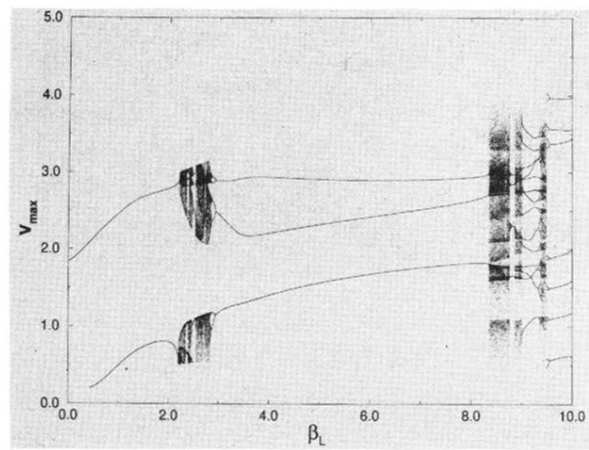
[35] R. L. Kautz, J. Appl. Phys. **58**, 424 (1985).

FIG. 2. A bifurcation diagram with β_L as the control parameter. The other parameters are fixed at $i = 1.20$ and $\beta_C = 0.707$.
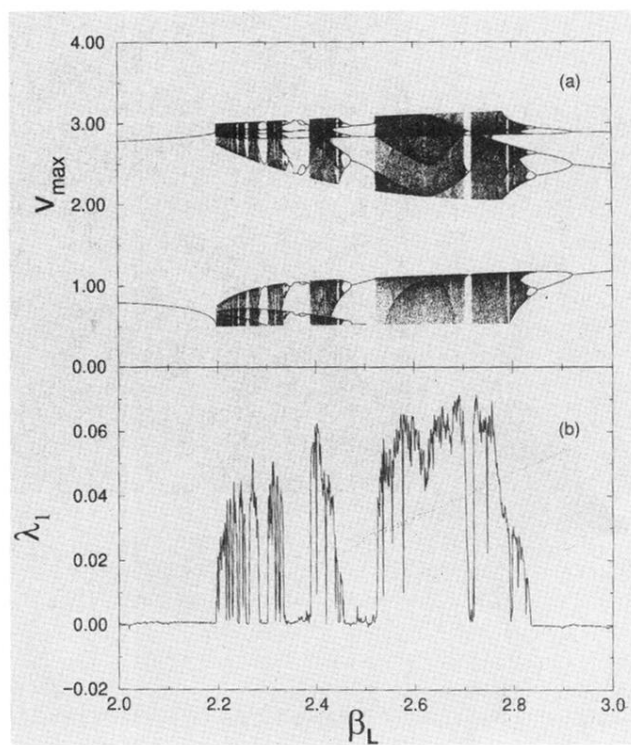
FIG. 3. (a) Detail of the bifurcation diagram of Fig. 2. (b) The corresponding largest Lyapunov exponent.
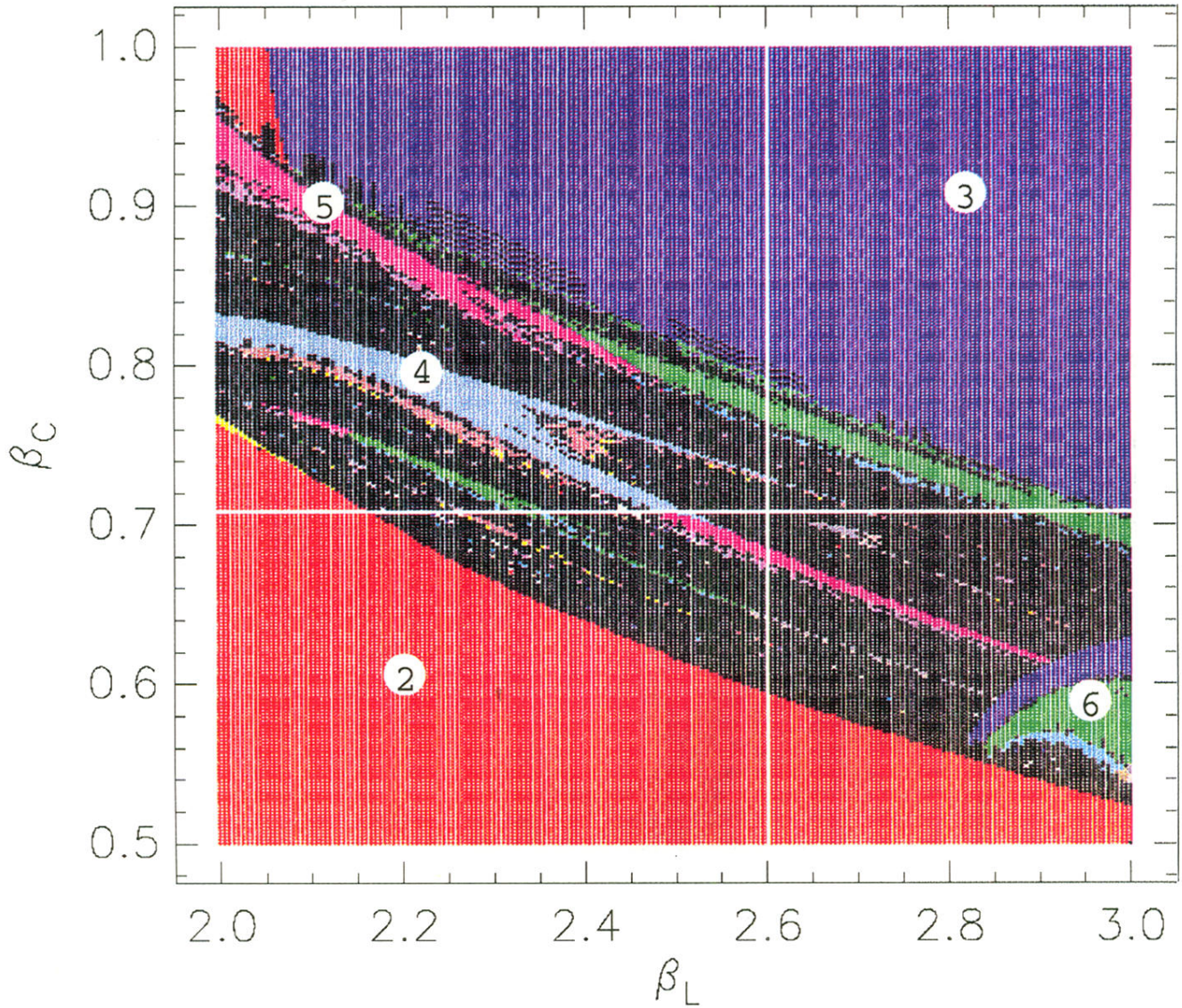
FIG. 4. A two-dimensional generalization of the bifurcation diagrams. Here the bias current is fixed at $i = 1.20$ and the other two parameters β_L and β_C are varied on a 250×200 grid. The color code for several low-periodicity solutions are indicated by the numbers in small circles. All solutions with periodicity higher than 20, including chaotic solutions, are marked black. The horizontal white line corresponds to the bifurcation diagram of Fig. 3(a).
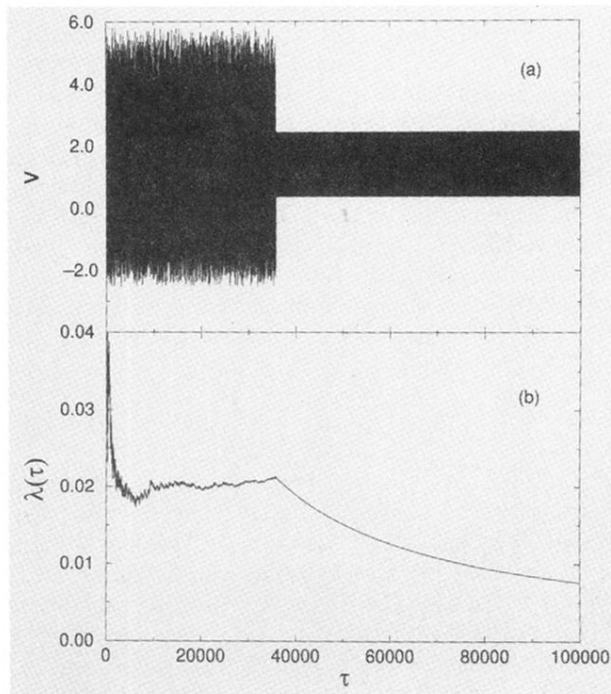
FIG. 5. A chaotic transient is illustrated here in the
voltage wave form (a), and also by the approximate Lya-
punov exponent $\lambda(\tau)$ (b).   The parameter values are
$\beta_L = 29.215, \beta_C = 0.707$, and $i = 1.25$. The lifetime of the
chaotic transient is $\tau_{\mathrm{tr}} \approx 36\,000$. Notice that as soon as the
trajectory reaches the periodic attractor, $\lambda(\tau)$ starts to decay
as $1/\tau$, eventually giving $\lambda_1 = 0$.